Applied Mathematical Modelling 33 (2009) 2207–2217

Contents lists available at ScienceDirect

Applied Mathematical Modelling

journal homepage: www.elsevier.com/locate/apm

Modeling the capacity of a novel flow-energy harvester

Qiang Zhu [a,*], Max Haase [b], Chin H. Wu [c]

[a] Department of Structural Engineering, UC San Diego, La Jolla, CA 92093-0085, USA
[b] Department of Mechanical Engineering and Marine Technology, University of Rostock, 18059 Rostock, Germany
[c] Department of Civil and Environmental Engineering, University of Wisconsin, Madison, WI 53706, USA

ARTICLE INFO

Article history:
Received 8 March 2007
Received in revised form 16 May 2008
Accepted 23 May 2008
Available online 7 July 2008

Keywords:
Oscillating foil
Flow energy harvester
Numerical modeling
Boundary element

ABSTRACT

The performance of a new type of flow energy harvester based on oscillating foils is investigated through numerical modeling by using two methods, a 2D thin-plate model and a 3D nonlinear boundary-element model. The fluid–structure interaction problem involved in the dynamics of a heaving/pitching foil coupled with an actuation/energy harvesting system in this device is examined. The 2D analysis allows us to simulate dynamics of the flapping-foil system over a large range of parameters and to identify areas of special interests (e.g., high energy output or high efficiency). In the vicinity of these areas the 3D model can accurately predict the performance of the system. By examining the power extraction capacity and efficiency of the system at various geometric, mechanical, and kinematic parameters, the optimal performance of the system is determined. In addition, the performance is found to be enhanced by the presence of a solid ground, as well as the thickness of the foil (at certain frequencies).

1. Introduction

With the increasing demand for energy and the decreasing supplies of fossil fuels, water current and wind are re-emerging as alternative sources of renewable energy. A typical design of a flow-energy harvester, the windmill, characterizes a number of blades with the rotation axis parallel to the incoming flow. This design may lead to large translational speed at the tips of the blades, causing environmental problems such as noise and hazard to birds.

In recent years, a new type of flow energy recovery paradigm based upon a novel flapping-foil technology has been proposed [1]. A prototype named Stingray was developed and tested [2]. The most distinctive feature of this new design is that it replaces the rotating blades of a conventional windmill by a foil undergoing unsteady motions. By varying the pitch angle of the foil periodically through a simple control/actuation mechanism, the new device was able to convert the responding heaving motion of the foil into electric energy.

The interest in flapping foils stems from biomimetic studies of the locomotion of aquatic animals and insects. Modeled after a fish fin or a insect wing, flapping foils were originally developed to be an efficient apparatus to generate propulsion force [3,4]. During its unsteady motions, a flapping foil is also able to produce significant lift force [5], a mechanism utilized in insect flying [6,7]. Other applications of flapping foils have also been explored. For example, both experimental [8] and analytical studies [9] showed that a submerged flapping foil was capable of generating thrust under free-surface waves in both head and following sea conditions.

Despite these studies on the dynamics of flapping foils, to date there exist very few studies on the capability of a flapping foil to directly harvest the kinetic energy of an incoming flow. Through experiments and two-dimensional numerical simulations,

* Corresponding author. Tel.: +1 858 822 2161; fax: +1 858 822 2260.
E-mail address: qizhu@ucsd.edu (Q. Zhu).

0307-904X/$ - see front matter © 2008 Elsevier Inc. All rights reserved.
doi:10.1016/j.apm.2008.05.027

Jones and Platzer [10] examined the energy exchange between a uniform flow and a foil undergoing prescribed pitching and plunging motions, and demonstrated the possibility of energy extraction. Performance enhancement was further shown *via* a double-foil tandem formation [11]. In their numerical studies, the foil motion was prescribed so that the coupled dynamics of the flapping foil, the energy generator, and the control/actuation system was not taken into account.

It is the primary objective of this study to carry out fully-coupled numerical investigations of the flapping-foil energy harvesting system and determine its feasibility, *i.e.*, the capability of energy generation over reasonably large parameter regions. Specifically we would like to determine the potential capacity and efficiency of the device. In contrast to previous studies, in which the motion of the foil was arbitrarily prescribed, we solve a fully coupled fluid–structure interaction problem to obtain the response of the foil. A dual-model approach, including a 2D thin-plate model and a 3D boundary-element model, is employed to map the behavior of the system over a wide range of mechanical and kinematic parameters, to achieve accurate prediction of the optimal performance, and to examine factors that may affect the performance of the system.

In Section 2, the physical model that represents the flapping-foil energy harvesting system will be described. It will also present the mathematical formulations and numerical issues of the 2D model and the 3D boundary-element method. Numerical results, including the comparison between 2D and 3D predictions are presented in Section 3. Finally, conclusions are given in Section 4.

2. Problem description and numerical approach

We focus on a case in which the foil has two degrees of freedom, heave and pitch. The pitch motion is prescribed, while the heave motion is determined through the interaction among the surround flow field, the foil, the supporting system (modeled as a spring), and the generator (modeled as a damper). The net power generation is evaluated as the difference between the power absorbed by the damper and the power required to rotate the foil.

2.1. Physical problem

As shown in Fig. 1, we consider a foil mounted on a spring-damper base in a uniform flow with velocity U. A Cartesian coordinate system (x, y, z) is employed with x in the direction of U and y in the direction of the span. A pitching motion is imposed and the pitch angle $\theta(t) = \theta_0 e^{i\omega t}$, where θ_0 is the pitching amplitude and ω the frequency of motion. The foil is free to heave in the vertical direction with $z = z(t)$. The pitching axis, which coincides with the position where the foil is attached to the spring-damper base, is located at a distance b behind the center of the foil (b is defined to be positive if the pitching axis is in the downstream side of the center). The chord length of the foil is a and the span is s. The spring is assumed to be linear with a spring constant k. The damper, which represents the energy extraction from the generator, is assumed to be viscous with a damping coefficient c.

The mass of the foil is assumed to be negligible compared to its added mass. The heaving motion of the foil is thus determined through

$$kz + c\dot{z} = F, \tag{1}$$

where F denotes the hydrodynamic lift force on the foil (including the added mass effect). By further assuming that the loss of mechanical energy through the damper c is completely converted into electric energy, the average power output is expressed as

$$P_o = \overline{c\dot{z}^2}. \tag{2}$$

To activate the pitch motion, an external moment M_a is imposed. By ignoring the rotational inertia of the foil and considering the balance of moments, we have $M_a = -M$, where M is the hydrodynamic moment on the foil. The average power spent to rotate the foil is given as

$$P_i = \overline{M_a\dot{\theta}^2}. \tag{3}$$

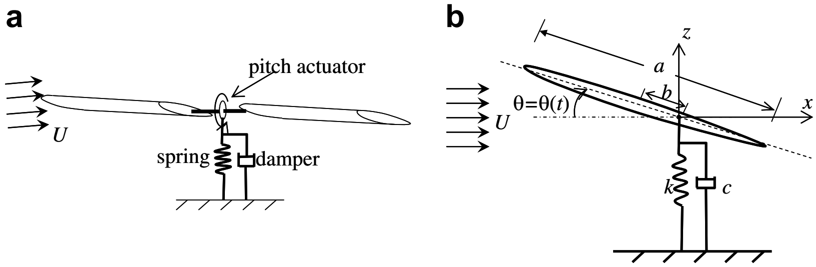

Fig. 1. (a) Schematic of the flapping-foil energy harvester. (b) Definition of symbols.

The net power generation is then determined as $P = P_o - P_i$. The corresponding efficiency, defined as the ratio between P and the energy flux of the incoming flow, is

$$\eta = \frac{P}{\rho U^3 sh}, \tag{4}$$

where h is the heaving amplitude. In order to accurately predict the net power P and the efficiency η, it is necessary to evaluate the hydrodynamic lift force F, as well as the hydrodynamic moment M.

2.2. Mathematical models

2.2.1. Two-dimensional model

The 2D model used in this study originates from the thin plate approximation by Theodorsen [12]. Using linear analysis, this model provides a closed-form solution of the hydrodynamic forces and moments on a zero-thickness plate undergoing harmonic oscillation in a uniform stream. In a generalized form, it can also be applied to study general unsteady motions of a plate [13]. Owing to its simplicity, it has been widely employed in the investigation of unsteady foil dynamics and flow-induced instability [14].

For a 2D zero-thickness flat plate undergoing small-amplitude harmonic oscillations $\theta = \theta_0 e^{i\omega t}$ and $z = z_0 e^{i\omega t}$, the hydrodynamic lift force is obtained as the combination of a quasi-steady lift force, an added mass force, and an adjustment due to wake effects. Summing up these components, the lift force is [15]

$$F = \pi a\rho UsC[-\dot{z} + U\theta + (a/4 - b)\dot{\theta}] + \frac{1}{4}\pi\rho sa^2(-\ddot{z} + U\dot{\theta} - b\ddot{\theta}), \tag{5}$$

where C is the lift deficiency factor, which denotes the wake-induced lift reduction. The natural frequency in the heave mode is $\omega_n = 2\sqrt{k/\pi\rho sa^2}$. Substituting Eq. (5) into Eq. (1), we have

$$z_0/\theta_0 = \frac{\pi\rho aUs[U + i\omega(a/4 - b)]C + \pi\rho a^2 s(i\omega U + b\omega^2)/4}{i\omega c + k - \pi\rho a[-i\omega UC + a\omega^2/4]s}. \tag{6}$$

With the heave amplitude given as $h = |z_0|$, the average power output in Eq. (2) is calculated as

$$P_o = c\omega^2 h^2/2, \tag{7}$$

indicating that the power extraction is scaled as θ_0^2. Similarly, the hydrodynamic moment on the foil with respect to the pitching axis is

$$M = -\frac{\pi\rho a^2 s}{4}\left\{b\ddot{z} + (a/4 - b)U\dot{\theta} + \frac{a^2}{4}\left(\frac{1}{8} + \frac{4b^2}{a^2}\right)\ddot{\theta} - UC(4b/a - 1)[-\dot{z} + U\theta + (a/4 - b)\dot{\theta}]\right\}. \tag{8}$$

Assuming that the rotational inertia of the foil is negligible, from the balance of moment we have $M_a = -M = M_0 e^{i\omega t}$. The average power spent to rotate the foil by activating the pitching motion through M_a is given as

$$P_i = \overline{M_a\dot{\theta}} = -\omega\theta_0 Im(M_0)/2. \tag{9}$$

The corresponding efficiency is therefore calculated using Eqs. (4), (7), and (9). Note that according to Theodorsen [12], the factor C in Eqs. (5) and (8) is

$$C(\sigma) = \frac{K_1(i\sigma)}{K_0(i\sigma) + K_1(i\sigma)} = \frac{H_1^{(2)}(\sigma)}{H_1^{(2)}(\sigma) + H_0^{(2)}(\sigma)}, \tag{10}$$

where $\sigma = \omega a/U$ is the reduced frequency. K_n $(n = 0, 1)$ is the modified Bessel function of the second kind, and $H_n^{(2)}$ $(n = 0, 1)$ is the Hankel function of the second kind. For computational purpose, we approximate the deficiency factor by a ratio of polynomials [16]:

$$C(\sigma) \approx \frac{(i\sigma)^3 a_3 + (i\sigma)^2 a_2 + (i\sigma)a_1 + a_0}{(i\sigma)^3 + (i\sigma)^2 b_2 + (i\sigma)b_1 + b_0}, \tag{11}$$

where $a_0 = 0.0451$, $a_1 = 0.5249$, $a_2 = 1.0761$, $a_3 = 0.5$, $b_0 = 0.0455$, $b_1 = 0.0699$, and $b_2 = 1.9022$.

2.2.2. Three-dimensional model

Based upon the potential-flow theory, the dynamics of the 3D foil motions is mathematically formulated through 3D boundary-integral equations. By using boundary elements, the method is applicable to arbitrarily-shaped bodies with fully nonlinear body motion and wake development. An application of this model to investigate the swimming process of aquatic creatures can be found in Zhu et al. [17]. The model successfully reproduced the experimentally observed and measured properties such as the reverse Kármán Vortex Street in the wake and the hydrodynamic loads on the bodies. Furthermore the model captures the near-body flow structures and complex wake–wake and wake–body interactions, demonstrating its capability to predict hydrodynamic performances of unsteady foils.

In this approach, the flow is assumed to be irrotational except for zero-thickness vorticity sheets in the wake. The flow potential $\Phi(\mathbf{x},t)$ ($\mathbf{x}=(x,y,z)$ represents an arbitrary point in space) is written as the linear superposition of two parts, $\Phi=\phi_b+\phi_w$, where ϕ_b represents the contribution from the foil body and ϕ_w the contribution from the wake. The problem is thus decomposed into two interdependent ones: the boundary value problem for ϕ_b, and the evolution of the wake which determines ϕ_w.

The boundary-value problem for ϕ_b consists of the Laplace equation $\nabla^2\phi_b=0$ inside the fluid domain, the far field condition $|\nabla\phi|\rightarrow 0$ as $|\mathbf{x}|\rightarrow\infty$, and the no-flux condition on the foil surface S_b:

$$\mathbf{n}\cdot\nabla\phi_b=\mathbf{n}\cdot[\mathbf{V}_b(\mathbf{x},t)-\nabla\phi_w], \tag{12}$$

where $\mathbf{V_b}$ is the instantaneous velocity of the foil, $\mathbf{n}$ is the unit normal vector pointing into the foil. The integral equation for is obtained by invoking the Green's theorem, at any point $\mathbf{x}=(x,y,z)$ on the foil surface we have

$$2\pi\phi_b(\mathbf{x},t)+\iint_{S_b}\phi_b(\mathbf{x}',t)\mathbf{n}'\cdot\nabla(1/|\mathbf{x}-\mathbf{x}'|)d\mathbf{x}'=\iint_{S_b}(1/|\mathbf{x}-\mathbf{x}'|)\mathbf{n}'\cdot\nabla\phi_b(\mathbf{x}',t)d\mathbf{x}'. \tag{13}$$

In Eq. (13), the left-hand side terms contain the unknown potential ϕ_b on S_b. The right-hand side term is known since the value of $\mathbf{n}\cdot\nabla\phi_b$ on S_b is given through Eq. (12).

To solve Eq. (13), a low-order boundary-element algorithm is applied to find the unknown body influence potential ϕ_b on S_b. The foil surface S_b is discretized into N_{bs} spanwise panels and N_{bc} chordwise panels. In addition, N_{bc} panels are added at each end of the span to close the tips. Therefore, the total number of body panels is $N_b=(N_{bs}+2)N_{bc}$. Within each panel S_{bj}, $j=1,\cdots,N_b$, the body potential ϕ_b and its normal derivative are assumed to be constants. By collocating at the centroids of the panels, Eq. (13) becomes a system of linear equations, and can be readily solved. With the value of ϕ_b on S_b thus determined, its value at any point $\mathbf{x}$ inside the fluid is evaluated through the Green's theorem, i.e.

$$\phi_b(\mathbf{x},t)=-\frac{1}{4\pi}\iint_{S_b}\phi_b(\mathbf{x}',t)\mathbf{n}'\cdot\nabla(1/|\mathbf{x}-\mathbf{x}'|)d\mathbf{x}'+\frac{1}{4\pi}\iint_{S_b}(1/|\mathbf{x}-\mathbf{x}'|)\mathbf{n}'\cdot\nabla\phi_b(\mathbf{x}',t)d\mathbf{x}'. \tag{14}$$

To determine ϕ_w, the wake is denoted by a distribution of dipoles on a sheet starting from the sharp trailing edge of the foil. The wake sheet elongates at every time step, representing the continuous shedding of vorticity from the trailing edge. The strength of newly shed wake is determined by the Kutta condition, either explicit or implicit. The explicit Kutta condition evaluates the new wake strength ϕ_w at the trailing edge as the instantaneous difference of body influence potential ϕ_b between the upper and lower surfaces near the edge [17]. The implicit Kutta condition, on the other hand, enforces a zero pressure difference condition across the trailing edge through Newton–Raphson iterations [18]. While the implicit Kutta condition is expected to be more accurate, it is computationally expensive owing to the evaluation of the Jacobian. In the present work, the explicit Kutta condition is therefore applied. The rest of the wake, treated as a material surface, is carried downstream by the collective effect of the upcoming flow and the self-induced velocity, and its strength is kept unchangeable due to the absence of dissipation. In order to stabilize the evolution of the discretely distributed vorticity in the wake, it is necessary to introduce a desingularization algorithm, in which we assign a finite core radius δ to each (body or wake) panel of dipole distribution. It has been demonstrated that the hydrodynamic forces on the body are not sensitive to the value of δ [17].

With the flow potential Φ given by summing up the body influence potential ϕ_b and the wake influence potential ϕ_w, the hydrodynamic force $\mathbf{F}_h$ on the body surface is readily determined through Bernoulli's equation, we have

$$\mathbf{F}_h=-\rho\iint_{S_b}\left\{\frac{\partial\Phi(\mathbf{x}',t)}{\partial t}+\frac{1}{2}|\nabla\Phi(\mathbf{x}',t)|^2\right\}\mathbf{n}'d\mathbf{x}'. \tag{15}$$

Similarly, the hydrodynamic moment $\mathbf{M}_h$ is given as

$$\mathbf{M}_h=-\rho\iint_{S_b}\left\{\frac{\partial\Phi(\mathbf{x}',t)}{\partial t}+\frac{1}{2}|\nabla\Phi(\mathbf{x}',t)|^2\right\}\mathbf{n}'\times(\mathbf{x}'-\mathbf{x}_r)d\mathbf{x}', \tag{16}$$

where $\mathbf{x}_r$ is the location of the reference point (rotation axis). The lift force F is the z-component of $\mathbf{F}_h$, and the pitch moment M is the y-component of $\mathbf{M}_h$.

To solve the coupled fluid–structure interaction problem, we employ an iteration scheme. In most cases only a few iteration steps are needed, provided that the time step Δt is sufficiently small. The procedure is outlined below:

Step 1. At any time t, we start from an initial guess that the vertical position of the foil z remains the same as the previous time step, $z_1=z(t-\Delta t)$;
Step 2. The hydrodynamic problem is solved based on z_1 and the updated pitch angle $\theta(t)$ to evaluate the lift force $F(t)$;
Step 3. Eq. (1), which governs the heaving motion of the foil, is numerically integrated to obtain the updated position z;
Step 4. If z is not sufficiently close to z_1, we set $z_1=z$ and repeat steps 2–4.

The boundary-element solver has been extensively validated through convergence tests and comparisons with other analytical, numerical, and experimental works [17,19]. To further demonstrate the validity and accuracy of the coupled 3D method, we perform convergence tests with respect to the numerical parameters, including the number of panels deployed

Table 1
Convergence of the power extraction P (normalized by P_{max}) with respect to the number of body panels using $\Delta t = T/128$

$N_{bs} \backslash N_{bc}$	10	20	40	80
10	0.403	0.322	0.349	0.358
20	0.390	0.310	0.338	0.346
40	0.381	0.303	0.332	0.340

Table 2
Convergence of the power extraction P (normalized by P_{max}) with respect to the time step using $N_{bs} = N_{bc} = 40$

$T/\Delta t$	32	64	128	256
	0.476	0.377	0.332	0.317

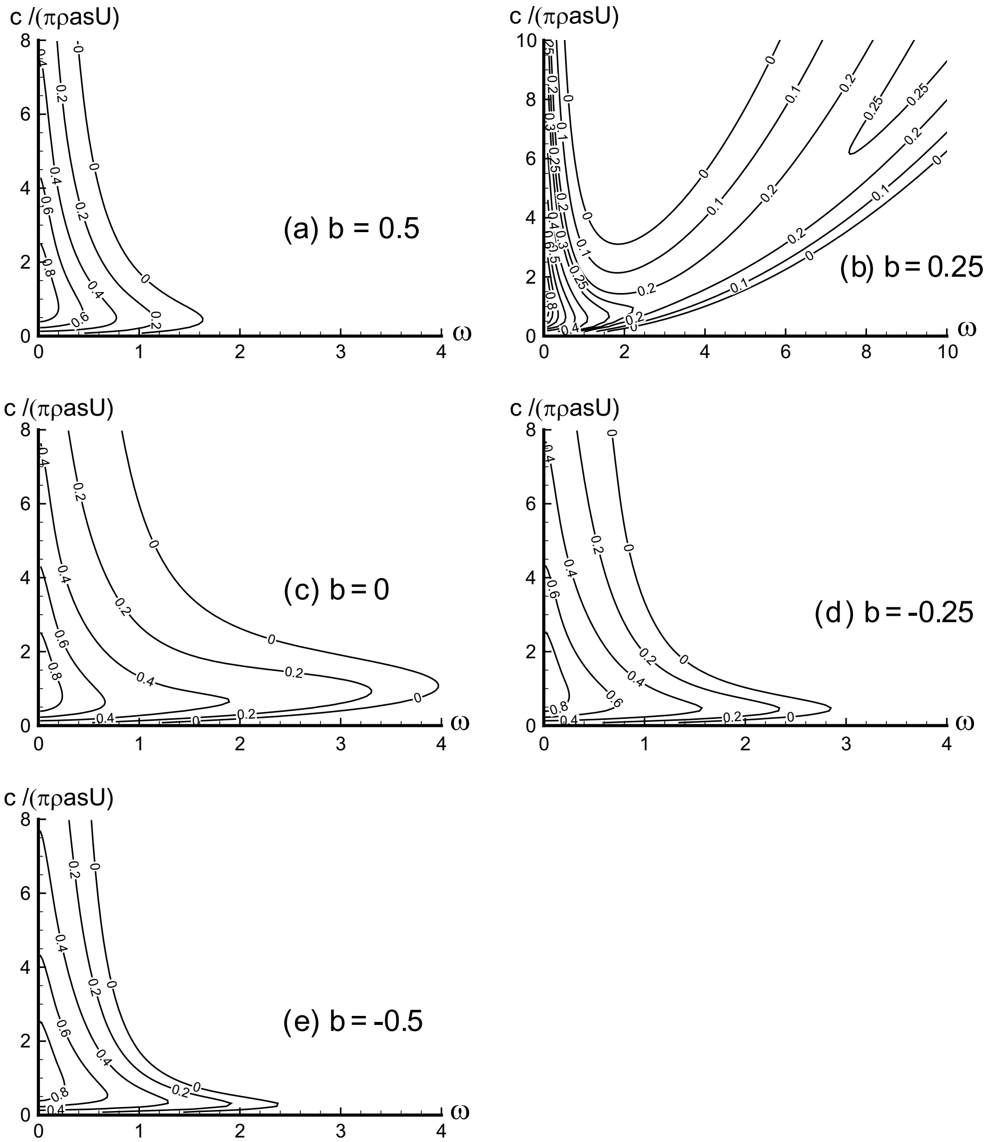

Fig. 2. Power extraction (divided by P_{max}) at $k = 0$ as functions of the frequency ω and the damping coefficient c.

on the foil surface N_{bs} and N_{bc}, as well as the time step Δt. In all the following computations, the problem is normalized by setting the chord length $a = 1$, the fluid density $\rho = 1$, and the speed of the incoming flow $U = 1$. For the convergence tests we consider a rectangular foil with NACA0005 cross-sections and aspect ratio $s/a = 10$. No spring is included so that $k = 0$. The pitching axis is located at the mid-chord ($b = 0$). The amplitude of pitch motion $\theta_0 = 10^\circ$, the frequency $\omega = 2$ (the corresponding period $T = \pi$), and the damping coefficient $c = 10\pi$. As shown in Tables 1 and 2, convergence is achieved with respect to N_{bs}, N_{bc}, and Δt. Based on these convergence tests, in the following computations $N_{bs} = N_{bc} = 40$ and $\Delta t = T/128$ are chosen. With these numerical parameters, the computational error is expected to be around 3%, which is sufficiently small for most applications.

3. Results

3.1. 2D results

We first apply the 2D model to evaluate the performance of the energy harvester. Unless otherwise specified, the pitching amplitude $\theta_0 = 10^\circ$ is chosen. Five different locations of the pitching axis ($b = -0.5, -0.25, 0, 0.25$, and 0.5) are examined.

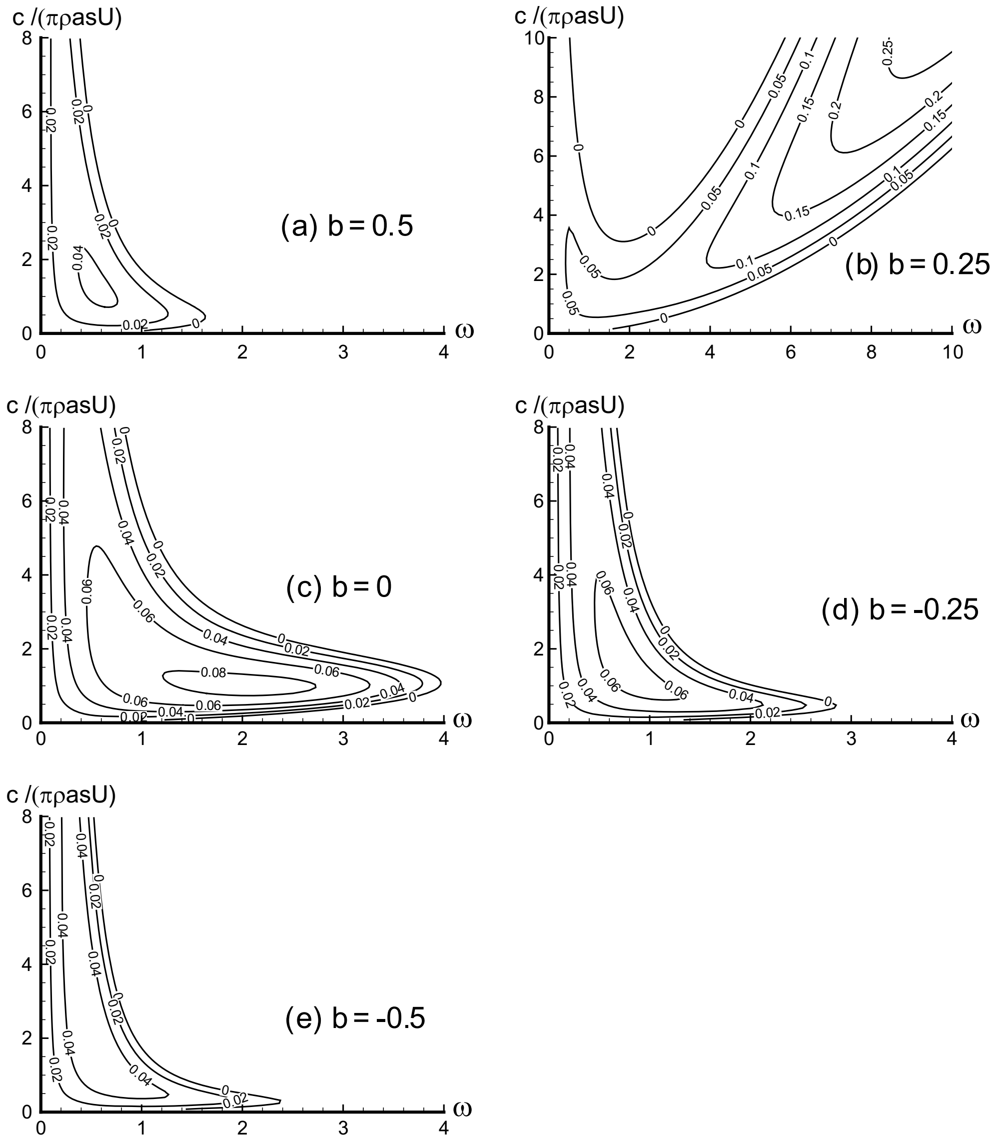

Fig. 3. Same as Fig. 2 but for efficiency η.

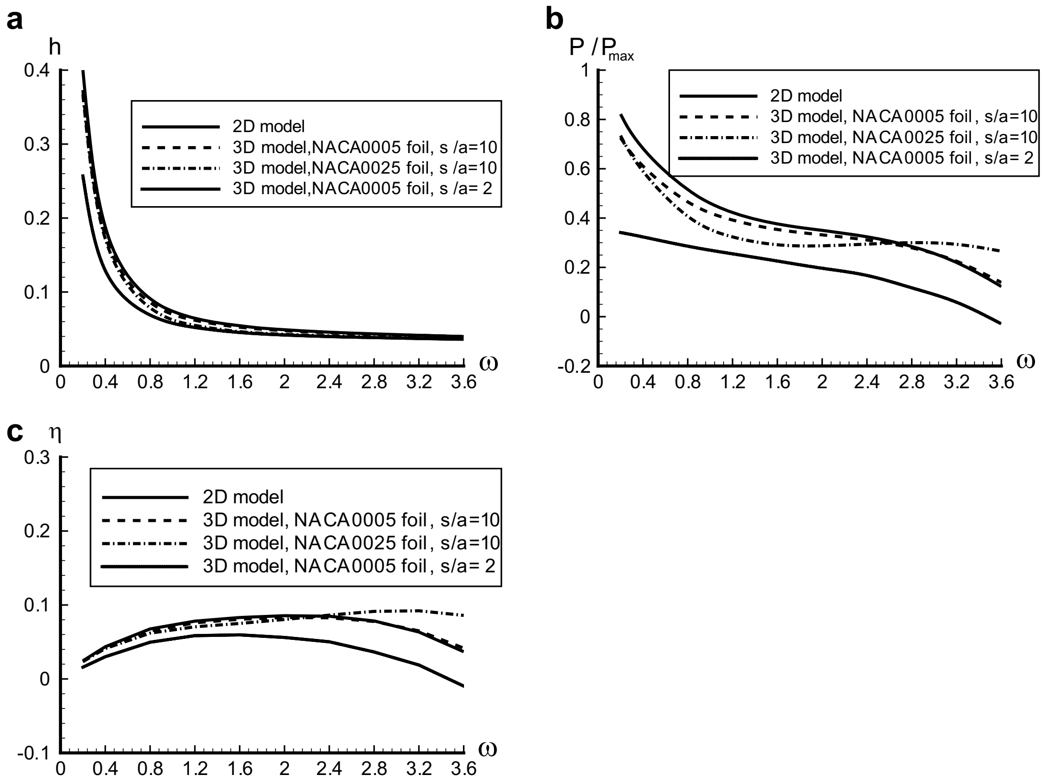

Fig. 4. (a) Heaving response, (b) power extraction, and (c) efficiency as functions of the frequency ω predicted by the 2D and the 3D models. $k = 0$, $b = 0$, $c = \pi\rho asU$, and $\theta_0 = 10^\circ$.

We start from the case $k = 0$, representing a system with no spring on the base. By considering $\omega \ll 1$, a low-frequency approximation of the solution is achieved and the maximum power extraction is

$$P_{\max} = \frac{\pi}{8}\rho asU^3\theta_0^2, \tag{17}$$

which is achieved at $c = \pi\rho asU$. The corresponding heaving amplitude and the efficiency are $h = U\theta_0/2\omega$ and $\eta = \pi a\theta_0\omega/4U$, respectively. Further simulations confirmed that the power extraction in Eq. (17) was also the maximum power extraction that can be obtained by the system for any b, k or ω. Figs. 2 and 3 show the power extraction P and the efficiency η as functions of the frequency ω and the damping coefficient c. When the pitching axis is located at the trailing edge ($b = 0.5$), positive P is observed at low frequencies ($\omega < 1.6$). The maximum power extraction is achieved in the vicinity of $\omega \sim 0$. The corresponding efficiency, on the other hand, only reaches 4% (at $\omega \approx 0.5$ and $c \approx 1.5$).

At $b = 0.25$, in low frequencies the performance of the system is similar to the case with $b = 0.5$. As the frequency increases, however, the system shows a peculiar behavior, characterized by monotonically increasing P and η as both ω and c increase. The maximum power extraction is about $0.28P_{\max}$ (achieved beyond the frequency range shown in Fig. 2), and the efficiency η keeps growing. Indeed, the results show that could even be larger than 1 in very large ω and c. This is attributed to the fact that the definition of η does not include the influence of pitching motion. This special case will be re-examined later with the more sophisticated boundary-element approach.

If the pitching axis is located at the mid-chord ($b = 0$), the leading edge ($b = -0.5$), or 1/4 chord length from the leading edge ($b = -0.25$), the performance of the system is qualitatively similar to the case when $b = 0.5$. Among these cases, the best performance is achieved at $b = 0$, with a maximum efficiency $\eta \approx 0.08$.

Cases with non-zero k's are also investigated. It is found that the region of positive P, denoting the range of parameters where power extraction from the incoming flow is possible, shrinks as k increases. The positive P regions will eventually disappear when k is sufficiently large.

To summarize, among all the cases we study, the best performance is obtained at $k = 0$ and $b = 0$ (mid-chord), where the power extraction P is close to $P_{\max}$ and the maximum η at $\theta_0 = 10^\circ$ is around 8%. According to our 2D model, η is linearly proportional to θ_0, indicating that higher efficiency is achieved by increasing θ_0. However, large θ_0 also leads to large heave motions, which may violate the linear model assumption of small-amplitude low-frequency motions for foils with small thickness and large span-to-chord ratios. To achieve more accurate predictions, in the following a 3D boundary-element model that incorporates the 3D geometry of the foil, nonlinear foil motion, and nonlinear wake evolution, is used to supplement the 2D model results. Owing to concerns about computational efforts, we will concentrate on the case corresponding to optimal performance at $k = 0$, $b = 0$, and $c = \pi\rho asU$. The case at $b = 0.25$, which is distinguished by its unique behavior, will also be re-examined. In addition, the effects of a solid ground will be addressed.

3.2. 3D results

To investigate the performance of the flapping-foil energy harvester with the boundary-element approach and compare with the 2D results, we focus on the optimal performance case ($k = 0$, $b = 0$), and the case in which the behavior of the system is different from others ($b = 0.25$). Fig. 4 displays the heaving amplitude h, the power extraction P, and the efficiency η of the system with a prescribed pitching amplitude $\theta_0 = 10^\circ$. Two different cross-sections, NACA0005 and NACA0025, are employed to demonstrate the effect of foil thickness. For a NACA0005 foil with $s/a = 10$, the predictions of both the amplitude h and the efficiency η are close to the 2D results. The power extraction P agrees with the 2D prediction at high frequency ($\omega > 2$), while insignificant discrepancy exists at low frequency, attributed to nonlinear effect associated with large heaving motion. The thickness of the foil is shown to decrease the power extraction/efficiency when $\omega < 2.8$, and increase them otherwise. The reduced aspect ratio ($s/a = 2$), on the other hand, decreases the heaving motion, the power extraction, and the efficiency in all the frequencies.

Despite the fact that in most cases with large aspect ratio and small foil thickness the 2D and the 3D predictions match quantitatively well with each other, discrepancies exist in certain parameters. The most notable case is at $k = 0$ and $b = 0.25$. For a close-up illustration, in Fig. 5 we plot the heaving amplitude h, the power output P_o, the power input P_i, and the net power extraction $P = P_o - P_i$ as functions of ω. The damping coefficient is chosen to be linearly proportional to ω and specified as $c = \pi\rho a^2 s\omega$ (corresponding to the bottom-left to upper-right diagonal line in Fig. 2b). As we see, the 2D and the 3D

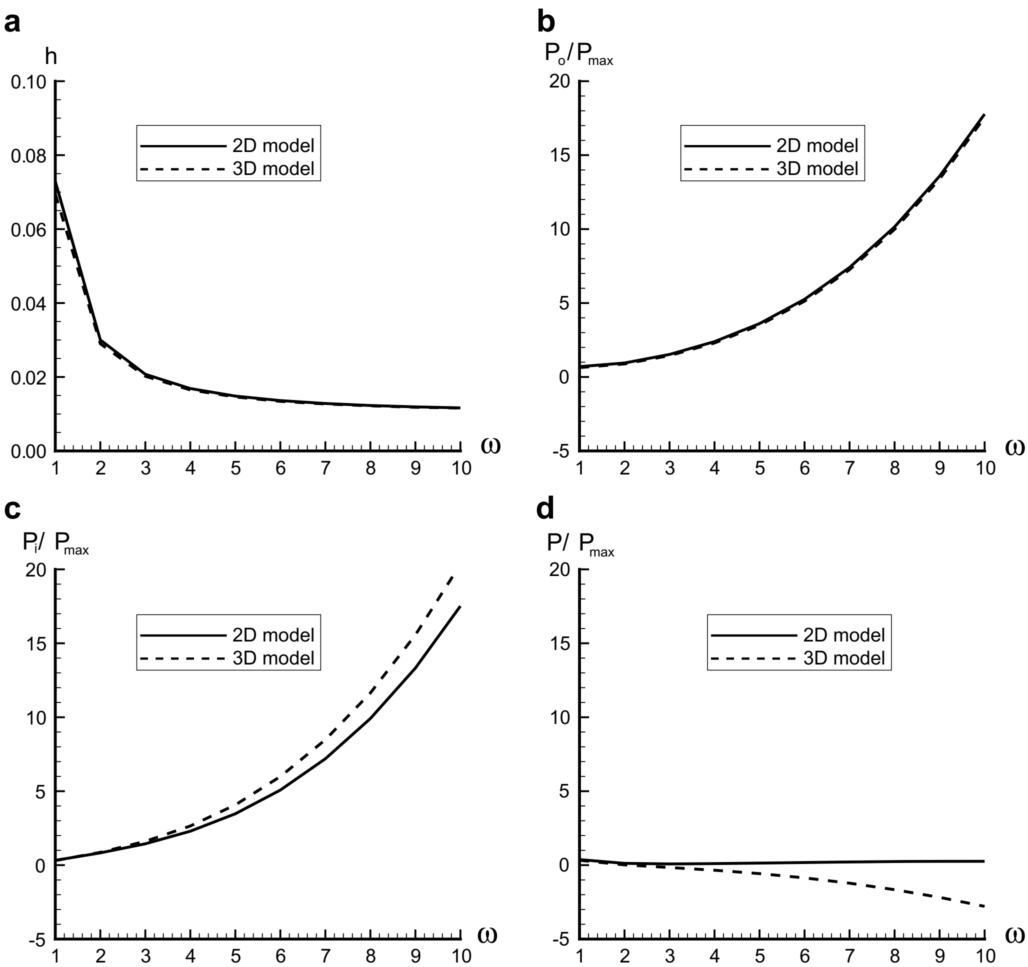

Fig. 5. (a) Heaving response, (b) power output, (c) power input, and (d) net power extraction as functions of the frequency ω for a NACA0005 foil predicted by the 2D and the 3D models. $k = 0$, $b = 0.25$, $c = \pi\rho a^2 s\omega$, $\theta_0 = 10^\circ$, and $s/a = 10$.

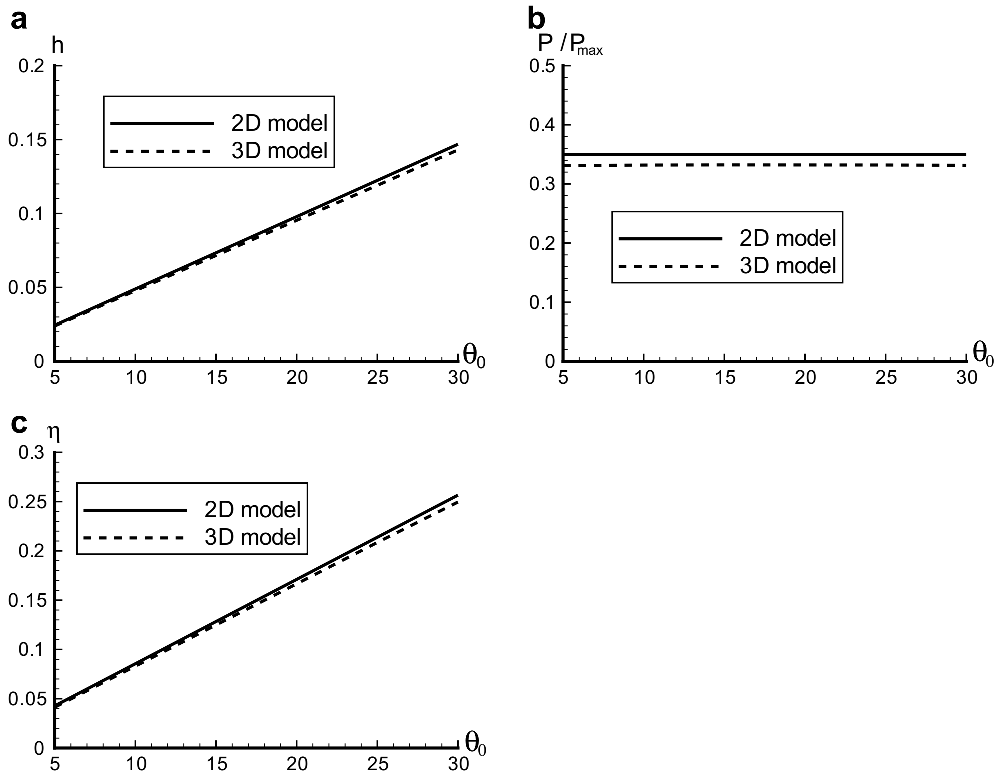

Fig. 6. (a) Heaving response, (b) power extraction, and (c) efficiency as functions of the pitching amplitude θ_0 (in degrees) predicted by the 2D and the 3D models for a NACA0005 foil with $k = 0$, $b = 0$, $c = \pi\rho a s U$, and $\omega = 2$.

models agree favorably with each other in terms of the predicted heaving amplitude h (Fig. 5a), and subsequently, the power output P_o (Fig. 5b). For the power consumption P_i, however, there exists considerable (but not large) difference between the two predictions (Fig. 5c). On the other hand, this particular case coincides with the scenario when $P_o \sim P_i \gg |P|$. As a result any relatively small discrepancies in P_i or P_o are amplified into a large discrepancy in P, as is shown in Fig. 5d. The specialty of this case is that although in the large ω region the 2D model predicts high performance of the system, the more accurate 3D model shows no power extraction.

Fig. 6 shows that at $\omega = 2$ and up until $\theta_0 = 30^\circ$, the h, P, and η predictions of 3D and 2D models are very close. The efficiency is almost linearly scaled with respect to θ_0.

4. Conclusions and discussion

A dual-model approach, including a 2D thin-plate model and a 3D boundary-element model, is employed to investigate the power extraction capacity of a flapping foil energy harvester consisting of a heaving–pitching foil coupled with a spring-damper base. The 2D model provides a leading-order estimate of the performance over a large range of mechanical and kinetic parameters, while the 3D model accurately predicts the dynamics of the system at the parameters where large power extraction capacity and large efficiency are found. Through systematic simulations using the 2D model, we found that the optimal performance of the system was achieved in the case when there is no spring, and when the pitching axis is located at the center of the chord. In this case, by using a thin foil with NACA0005 cross-sections and an aspect ratio of 10, the 3D boundary-element model delivers results that agree with the 2D predictions. We also found that the performance of the system was compromised by the three-dimensionality. The thickness of the foil increases the power production at higher frequencies. According to the 2D model, high performance is also achieved when the pitching axis is located at $\frac{1}{4}$ chord length from the trailing edge. This prediction, however, is proven to be spurious *via* the 3D model.

The accuracy of our models is affected by the potential flow approximation. In oscillating foils, the effect of viscosity is manifested in the formation and shedding of vortices near the leading edge (leading-edge separation). By visualizing the near-body flow field around a heaving–pitching foil, it has been shown that the strength of leading-edge separation is determined by the Strouhal number $S_t \equiv h\omega/\pi U$, as well as the maximum angle of attack $\alpha_{max} = |\theta - \tan^{-1}(\dot{z}/U)|_{max}$ [3]. The important finding is that at a moderate heave amplitude ($h/a \sim 1$), if the angle of attack is small ($\alpha_{max} < 7^\circ$) or if the Strouhal

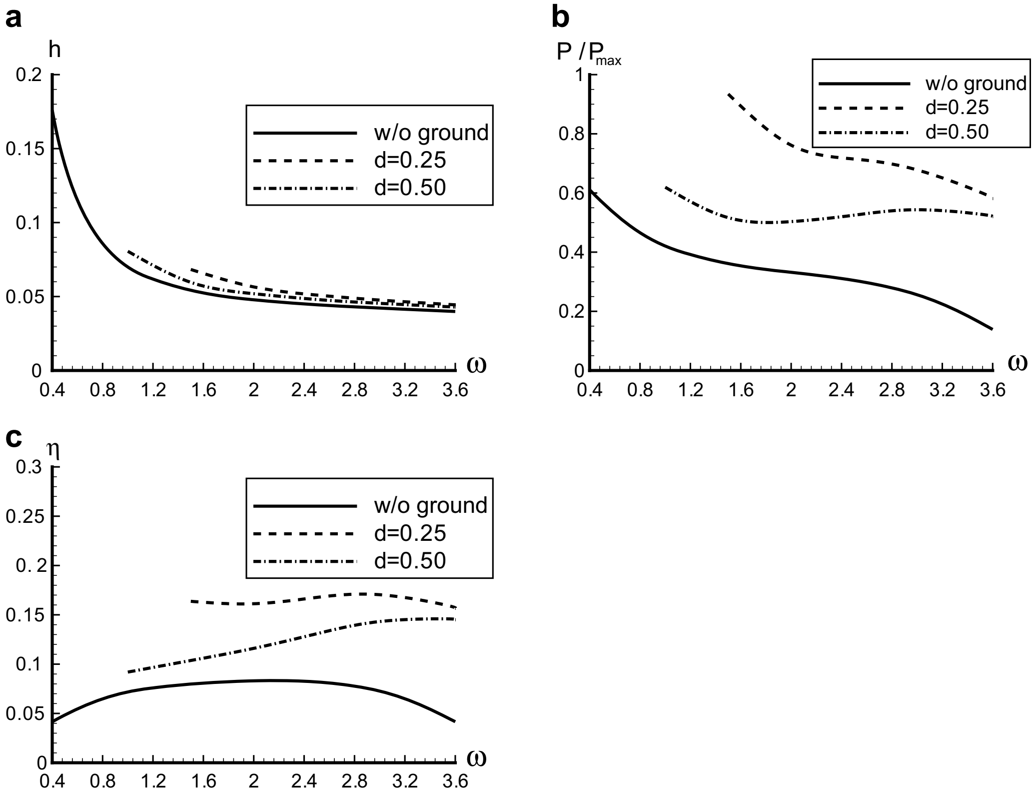

Fig. 7. (a) Heaving response, (b) power extraction, and (c) efficiency of the flapping foil energy harvester operating near a solid ground as functions of the frequency predicted by the 3D model for a NACA0005 foil $k = 0$, $b = 0$, $c = \pi\rho asU$, and $\theta_0 = 10^\circ$. d is the mean distance between the ground and the pitching axis.

number is small ($S_t < 0.12$), the vorticity generated near the leading edge can be neglected. Beyond these parameter regions, the leading-edge separation is distinguishably present. Indeed, within a certain range of parameters ($0.3 < S_t < 0.5$ and $13^\circ < \alpha_{max} < 36^\circ$), the flow field is dominated by vortices generated near the leading edge. In the same study, a potential-flow model was adopted and its prediction of hydrodynamic forces was consistent with experimental measurements up until $S_t \sim 0.3$, beyond which discrepancies were observed. To ensure that the influence of leading-edge separations can be neglected in our simulations (ref. Figs. 4–7), we examine the corresponding S_t and α_{max}. For $\theta_0 = 10^\circ$ and over the whole range of ω, we have $S_t < 0.05$ and $\alpha_{max} < 7^\circ$. As $\omega = 2$ and $\theta_0 \leqslant 30^\circ$, the maximum angle of attack increases beyond the threshold (7°), but the Strouhal number remains smaller than 0.1. These results suggest that the effect of leading-edge separation in our simulated cases is negligible. To summarize, by examining the range of Strouhal number and maximum angle of attack, the effect of leading-edge separation, which is not included in our numerical models, is found to be insignificant in the cases considered in this study.

Our simulations indicate that the maximum power extraction is $\pi\rho asU^3\theta_0^2/8$. For example, the power extracting capacity of a foil with a 1 m chord and a 10 m span in a 2 m/s water current is about 8.6 KW assuming that the pitching amplitude is 30°. At that pitching amplitude, the maximum efficiency is around 25%, which is low compared to the Betz coefficient (at around 59% it is theoretically the highest efficiency a windmill can achieve). One possible measure to increase the efficiency is to apply multiple foils in a tandem formation so that the downstream foils can further extract energy from the wake of the upstream foils, as suggested by Jones et al. [11]. Another measure is by simply putting the system close to the solid ground (sea floor) and utilizing the ground effect. In a steadily translational foil, it is known that the presence of a solid ground will increase the lift force, owing to the blocking of trailing vortices. Fig. 7 demonstrates the performance of the flapping-foil energy harvester with and without the ground effect. It is seen that the presence of the ground increases the heaving response of the foil, and greatly enhances both the power extraction and the efficiency. Indeed, in many cases the efficiency is doubled by the ground effect. We note that when the frequency of motion is small the heaving amplitude becomes so large that the foil may collide with the ground. These cases are subsequently ignored.

Acknowledgement

This study was supported by the University of California San Diego Academic Senate Research Fund.

References

[1] W. McKinney, J. DeLaurier, The wingmill: an oscillating-wing windmill, J. Energy 5 (2) (1981) 109–115.
[2] M. Campbell, Concept development of an oscillating tidal power generator, in: Proceedings of ASME Fluids Engineering Division Summer Meeting, Montreal, 2002.
[3] J.M. Anderson, K. Streitlien, D.S. Barret, M.S. Triantafyllou, Oscillating foils for high propulsive efficiency, J. Fluid Mech. 360 (1998) 41–72.
[4] M.S. Triantafyllou, A.H. Techet, F.S. Hover, Review of experimental work in biomimetic foils, IEEE J. Ocean Eng. 29 (3) (2004) 585–594.
[5] Z.J. Wang, Vortex shedding and frequency selection in flapping flight, J. Fluid Mech. 410 (2000) 323–341.
[6] H. Liu, K. Kawachi, A numerical study of insect flight, J. Comput. Phys. 146 (1998) 124–156.
[7] R. Rammamutri, W.C. Sandberg, A three-dimensional computational study of the aerodynamic mechanisms of insect flight, J. Exp. Biol. 205 (2002) 1507–1518.
[8] H. Isshiki, M. Murakami, Y. Terao, Utilization of wave energy into propulsion of ships – wave devouring propulsion, in: 15th Symposium On Naval Hydrodynamics, National Academy Press, Washington, DC, 1984, pp. 539–552.
[9] J. Grue, A. Mo, E. Palm, Propulsion of a foil moving in water waves, J. Fluid Mech. 186 (1998) 393–417.
[10] K.D. Jones, M.F. Platzer, Numerical computation of flapping-wing propulsion and power extraction, AIAA Paper No 97-0826, 1997.
[11] K.D. Jones, K. Lindsey, M.F. Platzer, An investigation of the fluid–structure interaction in an oscillating-wing micro-hydropower generator, Fluid Structure Interaction II, WIT Press, 2003. pp. 73–84.
[12] T. Theodorsen, General theory of aerodynamic instability and the mechanisms of flutter, National Advisory Committee for Aeronautics, Report No. 496, 1935.
[13] T. von Kárman, W.R. Sears, Airfoil theory for nonuniform motion, J. Aeronaut. Sci. 5 (10) (1938) 379–389.
[14] M.J. Lighthill, Aquatic animal propulsion of high hydromechanical efficiency, J. Fluid Mech. 44 (1970) 265–301.
[15] J. Katz, A. Plotkin, Low-Speed Aerodynamics: From Wing Theory to Panel Methods, McGraw-Hill, 1991.
[16] K.A. Harper, M.D. Berkemeier, S. Grace, Modeling the dynamics of spring-driven oscillating-foil propulsion, IEEE J. Ocean Eng. 23 (3) (1998) 285–296.
[17] Q. Zhu, M. Wolfgang, D.K.P. Yue, M.S. Triantafyllou, Three-dimensional flow structures and vorticity control in fish-like swimming, J. Fluid Mech. 468 (2002) 1–28.
[18] S.A. Kinnas, C-Y. Hsin, A boundary element method for the analysis of the unsteady flow around extreme propeller geometries, AIAA J. 30 (1992) 688–696.
[19] Q. Zhu, Y. Liu, D.K.P. Yue, Dynamics of a three-dimensional oscillating foil near the free surface, AIAA J. 44 (12) (2006) 2997–3009.